Design-Oriented Dissipativity Robustness Enhancement for Current Control of LCL-Filtered Grid-Following VSCs

He, Shan; Blaabjerg, Frede

Published in:
Proceedings of the 2023 IEEE Applied Power Electronics Conference and Exposition (APEC)

DOI (link to publication from Publisher):
10.1109/APEC43580.2023.10131261

Publication date:
2023

Document Version
Accepted author manuscript, peer reviewed version

Design-Oriented Dissipativity Robustness Enhancement for Current Control of LCL-Filtered Grid-Following VSCs

Shan He and Frede Blaabjerg
Department of Energy, Aalborg University
Aalborg 9220, Denmark
she@energy.aau.dk, fbl@energy.aau.dk

***Abstract*—Capacitor current active damping can effectively enhance dissipativity of current control for grid-connected voltage source converters. However, the dissipative characteristic of converter output admittance can easily be jeopardized by capacitor voltage feedforward and passive filter parameter deviation. To fill this gap, a design-oriented control scheme is proposed in this paper. First, a moving-average-filter-based filter is inserted in the capacitor voltage feedforward path to achieve the dissipativity near the switching frequency. Then, the capacitor current damping coefficient is designed based on the required passive filter parameter deviation. Finally, the effectiveness of the proposed scheme is verified through the experiments.**

***Keywords*—Grid-connected converter, current control, passive filter parameter deviation, dissipativity robustness, harmonic stability.**

I. INTRODUCTION

LCL-filtered grid-connected voltage source converters (VSC) are widely used in distributed generation systems based on photovoltaic, wind turbine, and energy storage systems [1]. Nevertheless, with the large-scale penetration of renewable generation, the grid admittance seen from the point of common coupling (PCC) varies in a wide range, which poses a significant challenge to the harmonic stability of the converter-grid system [2]. As an extension of the admittance shaping, the passivity-based current control is a promising solution to tackle the VSC-grid interactive instability challenge [3]. Specifically, only if the real part of the output admittance is non-negative for all frequencies, the stable operation can be secured regardless of the grid admittance [4]. However, pure passivity is impossible to obtain, and the upper boundary of the dissipative region is set to the Nyquist frequency [5].

Considering the digital current control, there is a control delay including the computation delay and the pulse width modulation (PWM) delay [6]. Further, a non-dissipative region will be induced by the control delay for the single-loop converter-side current control (interval between the critical frequency and the Nyquist frequency) and grid-side current control (interval between the critical frequency and the anti-resonant frequency) [7].

To mitigate the non-dissipative region, various damping methods have been proposed in the previous literature. Capacitor current active damping (CCAD) is an effective solution to enhance the dissipativity, and the damping coefficient is deduced based on the dissipative characteristic of the VSC output admittance at the critical frequency [8]. However, the passive filter parameter deviation can easily introduce a non-dissipative region near the critical frequency [9]. By replacing the damping coefficient with a digital filter, the dissipativity robustness can be enhanced [10-12]. But the anti-resonance frequency of the LCL filter shall be constrained to a specific range, which limits the design of the converter-side inductor and the filter capacitor. In addition, the PCC/filter capacitor voltage feedforward is often required in terms of the transients during the start-up and grid disturbances, but the dissipativity near the Nyquist frequency will be jeopardized if using unity feedforward [13-14].

To overcome the above-mentioned challenges, a low-pass filter is used in the capacitor voltage feedforward (CVF) path. Then the CCAD coefficient is designed based on the robustness against the required passive filter deviation. Finally, the proposed control method is validated through the experiments.

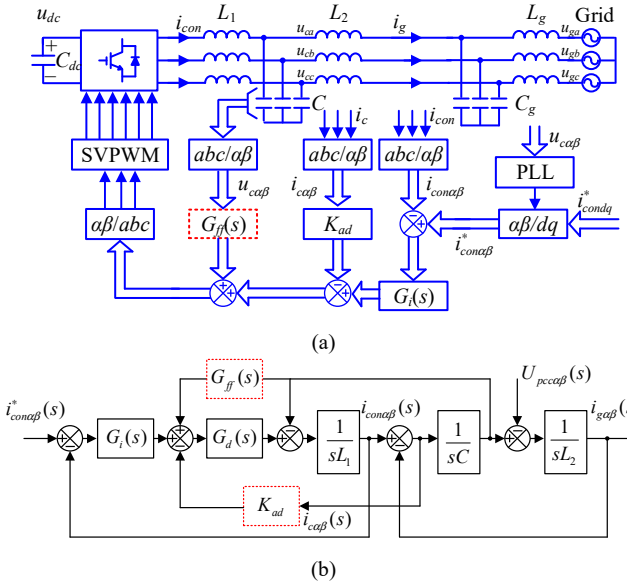

Fig. 1. Current control diagram of a three-phase grid-connected VSC. (a) Three-phase control diagram. (b) General current control model.

II. DISSIPATIVITY ROBUSTNESS ANALYSIS

The investigated three-phase grid-connected VSC with the converter-side current control is depicted in Fig. 1(a), where u_c is the filter capacitor voltage, u_{dc} is the dc-link voltage, i_{con} is the converter-side current, i_c is the filter capacitor current, L_1 is the converter-side inductance, L_2 is the grid-side inductor, C is the filter capacitor, and C_g and L_g are the grid impedance, respectively. i^*_{condq} and $i^*_{conαβ}$ are current references in the dq- and $αβ$-frame.

Regarding C and L_2 as part of the grid impedance, based on Fig. 1(b), the output converter-side current is

$$i_{con}(s) = G_{cl}(s)i_{con}^{*}(s) - Y_o(s)u_c(s) \tag{1}$$

where $G_{cl}(s)$ is the closed-loop transfer function between the reference current and the converter-side current, $Y_o(s)$ is the converter output admittance seen from the filter capacitor. The expressions of $G_{cl}(s)$ and $Y_o(s)$ are

$$G_{cl}(s) = \frac{G_d(s)G_i(s)}{sL_1 + G_d(s)G_i(s)} \tag{2}$$

$$Y_o(s) = \frac{1 + K_{ad}CsG_d(s) - G_{ff}(s)G_d(s)}{sL_1 + G_i(s)G_d(s)} \tag{3}$$

where K_{ad} is the CCAD coefficient, $G_{ff}(s)$ is the CVF function. $G_d(s)$ is the control delay including computation delay and PWM delay, which is given as

$$G_d(s) = e^{-1.5sT_{sa}}. \tag{4}$$

$G_i(s)$ is the proportional-resonant (PR) controller, which is

$$G_i(s) = K_p + K_r\omega_{rc}\frac{s\cos\varphi_g - \omega_g\sin\varphi_g}{s^2 + \omega_{rc}s + \omega_g^2} \tag{5}$$

where ω_g, ω_{rc}, φ_g, K_p, and K_r represent the grid fundamental angle frequency, the cut-off angle frequency of the resonant controller, the compensation angle of the resonant controller, the proportional and the resonant controller gain, respectively.

According to the passivity theory, a grid-connected VSC can be stabilized if the two constraints are satisfied [3]. First, the closed-loop transfer function $G_{cl}(s)$ should be stable, which can be guaranteed by setting a proper bandwidth. Second, the real part of $Y_o(j\omega)$ is non-negative below Nyquist frequency. Since the control delay mainly affects the dissipativity in the high-frequency range, the R controller can be neglected. Substituting '$s=j\omega$' into (3), the real part of converter output admittance only considering CCAD is

$$\mathrm{Re}\{Y_o(j\omega)\} = \frac{\overbrace{K_p\cos(\omega T_d)}^{\text{Single-loop control}} + \overbrace{K_{ad}L_1C\cos(\omega T_d)\omega^2}^{\text{CCAD}}}{(K_p\cos(\omega T_d))^2 + (\omega L_1 - K_p\sin(\omega T_d))^2}. \tag{6}$$

By changing the sign of $Re\{Y_o(j\omega)\}$ at the critical angle frequency ($2\pi/4T_d$), the CCAD coefficient is given as

$$K_{ad} = -\frac{4T_d^2K_p}{\pi^2L_{1n}C_n} \tag{7}$$

where L_{1n} and C_n are the nominal values of converter-side inductance and filter capacitance. Considering a general case of passive filter parameter deviations, i.e., $L_1=kL_{1n}$, $C=kC_n$, $\mathrm{Re}\{Y_o(j\omega)\}$ is given as

$$\mathrm{Re}\{Y_o(j\omega)\} = \frac{\overbrace{K_p\cos(\omega T_d)}^{\text{Single-loop control}} + \overbrace{k^2\frac{\omega^2}{\omega_{crit}^2}K_p\cos(\omega T_d)}^{\text{CCAD}}}{(K_p\cos(\omega T_d))^2 + (\omega L_1 - K_p\sin(\omega T_d))^2}. \tag{8}$$

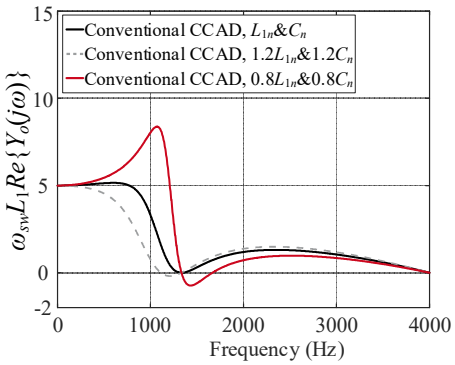

Fig. 2. Dissipativity robustness for double-sampling conventional CCAD.

Considering passive filter deviation, based on (8), the non-dissipative region only using CCAD is

$$f_{non-dissipative} = (f_{crit}, \frac{f_{crit}}{k}) \text{ or } (\frac{f_{crit}}{k}, f_{crit}) \tag{9}$$

where f_{crit} is the critical frequency. As shown in Fig. 2, the dissipativity around the critical frequency is weak even though there is no filter parameter deviation (k=1). Herein, double-sampling PWM is used and system specifications of the investigated grid-connected VSC are shown in Table I. Nevertheless, ±20% parameter deviation for passive filters is usually inevitable in the practical implementation. Further, −20% parameter deviation can introduce a larger non-dissipative region than +20% deviation, which can also be explained using (9).

To improve the transient performance under grid disturbance, a proportional CVF term is usually required in addition to the CCAD, which is

$$G_{ff}(s) = K_{ff} \tag{10}$$

where K_{ff} is the CVF coefficient. Then, the real part of converter output admittance considering CCAD and proportional CVF is

$$\mathrm{Re}\{Y_o(j\omega)\} = \frac{\overbrace{K_p\cos(\omega T_d)}^{\text{Single-loop control}} + \overbrace{k^2\frac{\omega^2}{\omega_{crit}^2}K_p\cos(\omega T_d)}^{\text{CCAD}}}{(K_p\cos(\omega T_d))^2 + (\omega L_1 - K_p\sin(\omega T_d))^2} + \frac{\overbrace{-K_{ff}K_p + K_{ff}L_1\sin(\omega T_d)\omega}^{\text{CVF}}}{(K_p\cos(\omega T_d))^2 + (\omega L_1 - K_p\sin(\omega T_d))^2}. \tag{11}$$

By substituting '$\omega=\omega_{crit}$' into (11), the dissipative characteristic at the critical frequency is

$$\mathrm{Re}\{Y_o(j\omega_{crit})\} = \frac{K_{ff}L_1(\omega_{crit} - \omega_c)}{(\omega_{crit}L_1 - K_p)^2} > 0. \tag{12}$$

where $\omega_c=K_p/L_1$ is the bandwidth of current controller. Recalling (4) and (9), the critical angle frequency ω_{crit} is $\frac{\omega_{sw}}{6}$ and $\frac{\omega_{sw}}{3}$ for the single-sampling PWM and double-sampling PWM, where is ω_{sw} the switching angle frequency. On the other hand, the bandwidth of current controller ω_c is usually set between $0.1\omega_{sw}$ to $0.2\omega_{sw}$ [15], and $\mathrm{Re}\{Y_o(j\omega_{crit})\}$ can always remain positive only if $\omega_{crit} > \omega_c$.

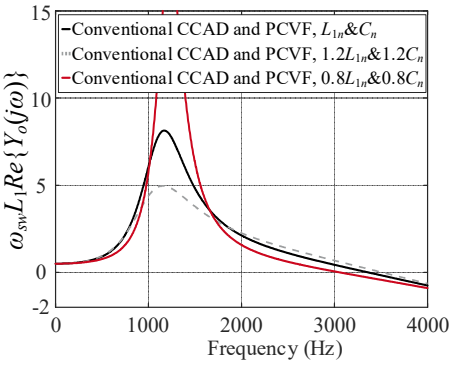

Fig. 3. Dissipativity robustness for double-sampling conventional CCAD and proportional CVF.

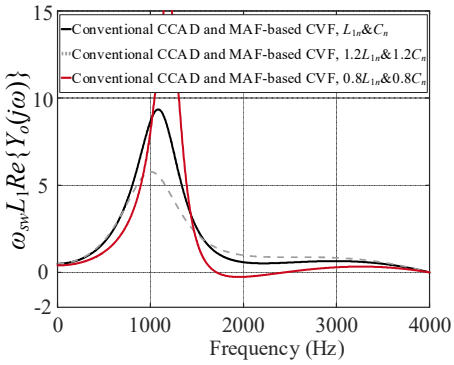

Fig. 4. Dissipativity robustness for double-sampling conventional CCAD and MAF-based CVF.

As illustrated in Fig. 3, the dissipativity robustness against the passive filter deviation near the critical frequency can be enhanced with the CVF. Note that the CVF coefficient should be lower than one to ensure the low-frequency dissipativity, and the value is set to 0.9 in this paper [13-14]. However, a non-dissipative region around the Nyquist angle frequency ($0.5\omega_{sa}$) is introduced, and the dissipative characteristic at the switching frequency is

$$\mathrm{Re}\{Y_o(j\omega_{sa})\}=\frac{-K_{ff}L_1(\omega_c+\omega_{sa})}{(\omega_{sa}L_1+K_p)^2}<0. \tag{13}$$

TABLE I. MAIN PARAMETERS OF GRID-CONNECTED CONVERTER

Symbol	Description	Value	Symbol	Description	Value
P_o	Output power	3 kW	u_g	Grid phase voltage (RMS)	220 V
u_{dc}	DC-link voltage	700 V	L_1	Converter-side inductance	4 mH
L_2	Grid-side inductance	2 mH	C	Filter capacitance	10 μF
f_{sa}	Sampling frequency	8 kHz	f_{sw}	Switching frequency	4 kHz
K_p	Proportional controller gain	20 Ω	K_r	Resonant controller gain	1000 Ω/s

III. DISSIPATIVITY ROBUSTNESS ENHANCEMENT

Recalling (11), the non-dissipative region around the Nyquist frequency is mainly related to '$\sin(0.5\omega_{sa}T_d)$'. To enhance the dissipativity around the Nyquist frequency when using proportional CVF, an extra $0.5T_{sa}$ delay can be added in the CVF path, and '$\sin(0.5\omega_{sa}(0.5T_{sa}+1.5T_{sa}))$' becomes zero. Note that the dissipativity at the Nyquist frequency can be further improved with a higher delay than $0.5T_{sa}$. In the practical implementation, a moving average filter (MAF) is used in the feedforward path, which is

$$G_{ff}(s)=K_{ff}(0.5+0.5e^{-sT_{sa}}). \tag{14}$$

Substituting (14) into (3), the real part of converter output admittance is given in (15). As shown in Fig. 4, the dissipativity around the switching frequency is enhanced, but another non-dissipative region is introduced when considering −20% passive filter parameter deviation (see red solid curve). It can be seen from (15) that the effect of filter parameter deviation on the dissipativity is mainly caused by the term '$k^2\frac{\omega^2}{\omega_{crit}^2}K_p\cos(\omega T_d)$', a CCAD correction term m^2 is further proposed to enhance the dissipativity.

$$\mathrm{Re}\{Y_o(j\omega)\}=\frac{\overbrace{K_p\cos(\omega T_d)}^{\text{Single-loop control}}+\overbrace{k^2\frac{\omega^2}{\omega_{crit}^2}K_p\cos(\omega T_d)}^{\text{CCAD}}}{(K_p\cos(\omega T_d))^2+(\omega L_1-K_p\sin(\omega T_d))^2}$$
$$\frac{\overbrace{-0.5K_{ff}K_p-0.5K_{ff}K_p\cos(\frac{2}{3}\omega T_d)}^{\text{CVF}}}{(K_p\cos(\omega T_d))^2+(\omega L_1-K_p\sin(\omega T_d))^2} \tag{15}$$
$$\frac{\overbrace{+0.5K_{ff}L_1\sin(\omega T_d)\omega+0.5K_{ff}L_1\sin(\frac{5}{3}\omega T_d)\omega}^{\text{CVF}}}{(K_p\cos(\omega T_d))^2+(\omega L_1-K_p\sin(\omega T_d))^2}.$$

Specifically, m is set to 0.8 considering an -20% parameter deviation. In addition, m can be designed to lower values in terms of the larger parameter deviation. Interestingly, the dissipativity can be still achieved under a +20% parameter deviation when m is 0.8. The corrected CCAD coefficient is

$$K_{ad}=-\frac{4T_d^2K_p}{\pi^2L_{1n}C_nm^2} \tag{16}$$

Substituting (14) and (16) into (3), the real part of the converter output admittance is given in (17). With the proposed method, it can be seen from Fig. 5 that not only the dissipativity around the switching frequency is achieved, but also the dissipativity robustness against the passive filter deviation is enhanced.

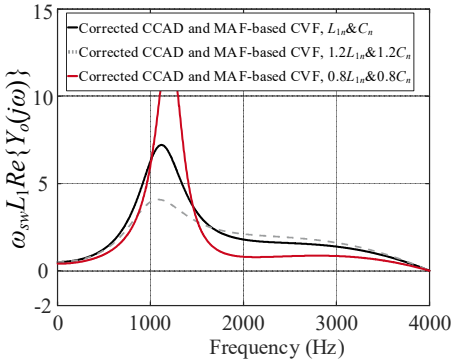

Fig. 5. Dissipativity robustness for double-sampling corrected CCAD and MAF-based CVF.

$$\mathrm{Re}\{Y_o(j\omega)\}=\frac{\overbrace{K_p\cos(\omega T_d)}^{\text{Single-loop control}}+\overbrace{\frac{k^2}{m^2}\frac{\omega^2}{\omega_{crit}^2}K_p\cos(\omega T_d)}^{\text{CCAD}}}{(K_p\cos(\omega T_d))^2+(\omega L_1-K_p\sin(\omega T_d))^2}$$
$$\frac{\overbrace{-0.5K_{ff}K_p-0.5K_{ff}K_p\cos(\frac{2}{3}\omega T_d)}^{\text{CVF}}}{(K_p\cos(\omega T_d))^2+(\omega L_1-K_p\sin(\omega T_d))^2} \quad (17)$$
$$\frac{\overbrace{+0.5K_{ff}L_1\sin(\omega T_d)\omega+0.5K_{ff}L_1\sin(\frac{5}{3}\omega T_d)\omega}^{\text{CVF}}}{(K_p\cos(\omega T_d))^2+(\omega L_1-K_p\sin(\omega T_d))^2}.$$

IV. Experimental Results

To further verify the theoretical analysis, experiments are carried out on a three-phase grid-connected VSC with an LCL filter, as shown in Fig. 6. The grid is emulated with a high-fidelity linear amplifier APS 15000. The applied half-bridge module and the control platform are a PEB-SiC-8024 module and a B-BOX RCP control platform from Imperix, respectively. The parameter of the three-phase grid-connected VSC with LCL-Filter is presented in Table I.

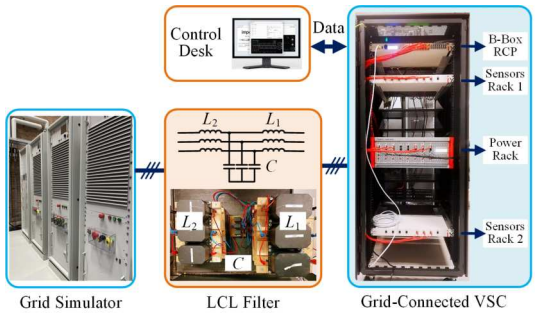

Fig. 6. A down-scaled grid-connected VSC with an LCL filter.

A. Robustness of conventional CCAD

To validate the dissipativity robustness of conventional CCAD, two cases are considered with/without a −20% deviation of nominal values of L_1 and C. Under an ideal grid condition, L_2 and C are regarded as the equivalent grid admittance $Y_{g,eq}(s)=1/sL_2+sC$. Bode plots of $Y_o(s)$ and $Y_{g,eq}(s)$ are presented in Fig. 7. If there is no parameter deviation, the system is stable. However, if there is a parameter deviation, $Y_{o,2}(s)$ intersects with $Y_{g,eq2}(s)$ in the negative-real-part region, which leads to a −2.9° phase margin (PM) and destabilizes the system..

The experimental result using conventional CCAD is shown in Fig. 8(a). The VSC starts at 40 ms, and the dc-link capacitor is charged to 700 V in the next 40 ms. Note that the start-up current is large since the grid voltage feedforward is not used. The reference current steps from 0 A to 15 A (rated current) at 80 ms. The VSC starts at 40 ms, and the dc-link capacitor is charged to 700 V in the next 40 ms. The reference current steps from 0 A to 15 A (rated current) at 80 ms. It can be seen in Fig. 8(b) that the VSC system becomes unstable due to the parameter deviation, which is consistent with the theoretical analysis in Fig. 7.

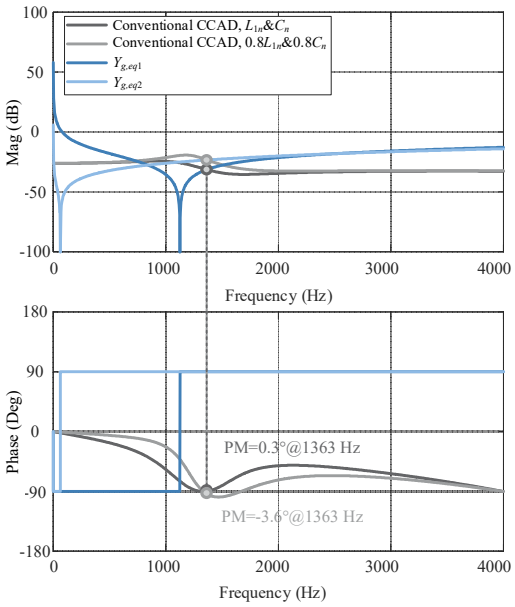

Fig. 7. Conventional CCAD dissipativity robustness assessment with a −20% deviation of L_1 and C. ($Y_{g,\,eq1}$: equivalent grid admittance without parameter deviation, $Y_{g,\,eq2}$: equivalent grid admittance with parameter deviation.)

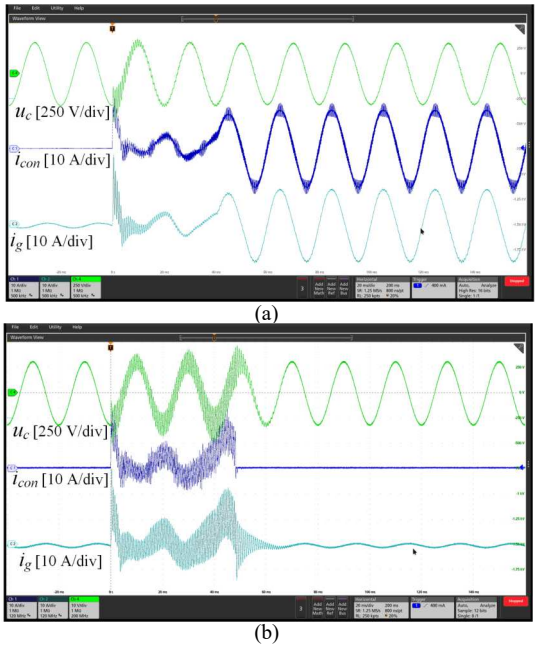

Fig. 8. Experimental results under an ideal grid condition. (a) Double-sampling conventional CCAD without parameter deviation. (b) Double-sampling conventional CCAD with a −20% deviation of L_1 and C.

B. Robustness of corrected CCAD and MAF-based CVF

When considering a −20% deviation of nominal values of L_1 and C and the capacitive grid simultaneously, as shown in Fig. 9, the system still cannot be stabilized for the conventional CCAD and MAF-based CVF (PM=−4.4°). After implementing the corrected CCAD, the system becomes stable because the dissipativity is achieved in the whole frequency range. As shown in Fig. 10, the proposed method can maintain stability and achieve high robustness, which is consistent with the analysis in Fig. 9.

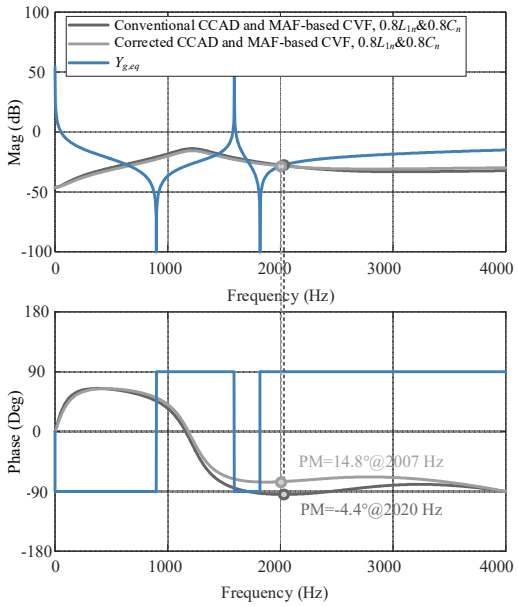

Fig. 9. Corrected CCAD and MAF-based CVF dissipativity robustness assessment with a −20% deviation of L_1 and C under a capacitive grid (L_g=1 mH and C_g=15 μF).

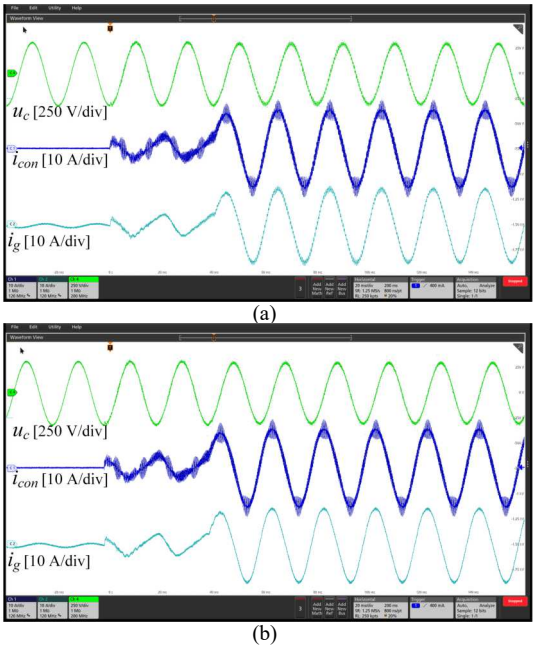

Fig. 10. Experimental results under a combination of L_g and C_g (L_g=1 mH and C_g=15 μF). (a) Double-sampling conventional CCAD and MAF-based CVF with a −20% deviation of L_1 and C. (b) Double-sampling corrected CCAD and MAF-based CVF with a −20% deviation of L_1 and C.

V. CONCLUSIONS

This paper investigates the dissipativity robustness against passive filter parameter deviation for LCL-filtered grid-connected VSCs. When only using CCAD, the dissipativity near the critical frequency is vulnerable if there is a filer parameter deviation. If adding proportional CVF, the dissipativity near the switching frequency cannot be satisfied. To tackle this challenge, a low-pass-filter-based CVF is used to enhance the dissipativity near the switching frequency, which can also improve the transient performance. Further, a CCAD correction term is proposed to enhance the dissipativity robustness against filter parameter deviation. Finally, the proposed method is validated through experiments.

ACKNOWLEDGMENT

This work was supported by the Reliable Power Electronics-Based Power System (REPEPS) project at the Department of AAU Energy, Aalborg University, as a part of the Villum Investigator Program funded by the Villum Foundation.

REFERENCES

[1] F. Blaabjerg, Y. Yang, D. Yang, and X. Wang, "Distributed power generation systems and protection," *Proc. IEEE*, vol. 105, no. 7, pp. 1311-1331, July 2017.

[2] X. Wang and F. Blaabjerg, "Harmonic stability in power electronic-based power systems: concept, modeling, and analysis," *IEEE Trans. Smart Grid*, vol. 10, no. 3, pp. 2858-2870, May 2019.

[3] L. Harnefors, X. Wang, A. Yepes, and F. Blaabjerg, "Passivity-based stability assessment of grid-connected VSCs-An overview," *IEEE J. Emerg. Sel. Top. Power Electron*., vol. 4, no. 1, pp. 116–125, Mar. 2016.

[4] L. Harnefors, A. Yepes, A. Vidal, and J. Gandoy, "Passivity-based controller design of grid-connected VSCs for prevention of electrical resonance instability," *IEEE Trans. Ind. Electron*., vol. 62, no. 2, pp. 702-710, Feb. 2015.

[5] L. Harnefors, R. Finger, X. Wang, H. Bai, and F. Blaabjerg, "VSC input-admittance modeling and analysis above the Nyquist frequency for passivity-based stability assessment," *IEEE Trans. Ind. Electron*., vol. 64, no. 8, pp. 6362–6370, Aug. 2017.

[6] J. Ma, X. Wang, F. Blaabjerg, L. Harnefors, and W. Song, "Accuracy analysis of the zero-order hold model for digital pulse width modulation," *IEEE Trans. Power Electron.*, vol. 33, no. 12, pp. 10826-10834, Dec. 2018.

[7] X. Wang, F. Blaabjerg, and P. Loh, "Passivity-based stability analysis and damping injection for multiparalleled VSCs with LCL filters," *IEEE Trans. Power Electron*., vol. 32, no. 11, pp. 8922-8935, Nov. 2017.

[8] C. Xie, K. Li, J. Zou, and J. Guerrero, "Passivity-based stabilization of LCL-type grid-connected inverters via a general admittance model," *IEEE Trans. Power Electron*., vol. 35, no. 6, pp. 6636-6648, 2020.

[9] S. He, Z. Yang, D. Zhou, X. Wang, R. De Doncker, and F. Blaabjerg, "Dissipativity robustness enhancement for LCL-filtered grid-connected VSCs with multi-sampled grid-side current control," *IEEE Trans. Power Electron.*, *early access*, 2022.

[10] X. Wang, Y. He, D. Pan, H. Zhang, Y. Ma, and X. Ruan, "Passivity enhancement for LCL-filtered inverter with grid current control and capacitor current active damping," *IEEE Trans. Power Electron*., vol. 37, no. 4, pp. 3801-3812, April 2022.

[11] H. Chen, P. Cheng, X. Wang, and F. Blaabjerg, "A passivity-based stability analysis of the active damping technique in the offshore wind farm applications," *IEEE Trans. Ind. Appl*., vol. 54, no. 5, pp. 5074-5082, Oct. 2018.

[12] S. Li, H. Lin, "A capacitor-current-feedback positive active damping control strategy for LCL-type grid-connected inverter to achieve high robustness," *IEEE Trans. Power Electron*., vol. 37, no. 6, pp. 6462-6474, June 2022.

[13] C. Wang, X. Wang, Y. He, and X. Ruan, "A passivity-based weighted proportional-derivative feedforward scheme for grid-connected inverters with enhanced harmonic rejection ability," *IEEE J. Emerg. Sel. Top. Power Electron.*, *early access*, 2022.

[14] S. He, D. Zhou, X. Wang, and F. Blaabjerg, "Passivity-based multisampled converter-side current control of LCL-filtered VSCs," *IEEE Trans. Power Electron.*, vol. 37, no. 11, pp. 13848-13860, Nov. 2022.

[15] D. Zhou and F. Blaabjerg, "Bandwidth oriented proportional-integral controller design for back-to-back power converters in DFIG wind turbine system," *IET Renew. Power Gener*., vol. 11, no. 7, pp. 941-951, June 2017.